We are IntechOpen, the world's leading publisher of Open Access books Built by scientists, for scientists

4,800
Open access books available

122,000
International authors and editors

135M
Downloads

Our authors are among the

154
Countries delivered to

TOP 1%
most cited scientists

12.2%
Contributors from top 500 universities

CLARIVATE ANALYTICS BOOK CITATION INDEX INDEXED

WEB OF SCIENCE™

Selection of our books indexed in the Book Citation Index in Web of Science™ Core Collection (BKCI)

Interested in publishing with us?
Contact book.department@intechopen.com

Numbers displayed above are based on latest data collected.
For more information visit www.intechopen.com

8

Numerical Simulation of Liquid-structure Interaction Problem in a Tank of a Space Re-entry Vehicle

Edoardo Bucchignani, Giuseppe Pezzella and Alfonso Matrone
Centro Italiano Ricerche Aerospaziali, via Maiorise, 81043 Capua
Italy

1. Introduction

The current perspectives in the aerospace sector require a particular attention for the analysis of several phenomena involving the coupling between the mechanical behaviour and the other physics fields such as the fluid-structure interaction problem. This issue is particularly felt in the design of Reusable Launch Vehicle (RLV) since, during reentry, such kind of vehicles carries large quantities of Main Engine Cut Off (MECO) residual propellants. The management of the residual propellant remaining in the reusable stage after MECO during a nominal mission is a crucial point for the design with respect to: dimensioning and weight, landing safety issues, and post-landing procedures.
Generally speaking, the motion of a fluid inside the RLVs' tank (e.g. propellant sloshing) can affect the stability of the spacecraft and, when it is too much violent, could damage the structure, generating the vehicle failure. As a consequence, the structural design of propellant tanks should take adequately into account for the propellant slosh load in combination with all other loads and inputs. Therefore, there is a need for explaining what happens with a fluid subjected to loading environment of a typical RLV reentry trajectory (Bucchignani et al. 2008). Sloshing of propellants describes the free-surface oscillations of a fluid in a partially filled tank. These oscillations are due to lateral and longitudinal or angular motions of the spacecraft, as well as, when there are no tank disturbances, to the interchange of kinetic energy and the potential energies due to gravitational and surface tension forces (NASA, 1968). In particular, these free oscillations may persist since the damping provided by the wiping of the fluid against the tank's wall is negligible. Therefore, forced oscillations result in large free-surface waves. The magnitude of propellant sloshing depends upon the following parameters: acceleration field, propellant properties, tank geometry, effective dumping, height of propellant in the tank, and perturbing motion of the tank (NASA, 1968).
In recent times, the phenomenon of sloshing in partially filled tanks has been widely investigated by means of analytical methods or experimental techniques. The problem of small horizontal oscillations has been extensively investigated in the past, using analytical and experimental methods (Faltinsen et al., 2000) (Faltinsen et al., 2001). It has been shown that the response is the same as that of the undamped Duffing equation and changes from soft-spring (decreasing amplitude with increasing frequency) to hard-spring (increasing

amplitude with increasing frequency) behaviour as the ratio width–depth passes through a certain value. This value has analytically been determined (Faltinsen, 1974) and is given by *L/H* = 0.3374. On the other side, there is a lack in numerical simulations based on Computational Fluid Dynamics (CFD) codes, because they often require large amount of computational resources.

The goal of this chapter is to describe an innovative numerical method, based on a *multiphysics* approach, aimed to the simulation of an unsteady RLV-like tank configuration, such as liquid Oxygen (LO_2) and/or liquid Hydrogen (LH_2), subject to a typical reentry loading environment. The flow-field pressure and the stress field in the tank structure have been evaluated considering the motion of an incompressible fluid with a mobile free surface, in a tank with deforming walls under the action of the liquid pressure. An unsteady Finite Element formulation is used, instead, for modelling the tank. The global solution procedure uses a *multiphysics approach*, which allows to simultaneously simulate all the fields involved in order to capture the physical effects arising from the interaction phenomena. In particular, the coupling algorithm, based on a *semi-implicit staggered method*, belongs to the class of the partition treatment techniques, which allow solving the fluid and structural fields by means of two distinct models.

This paper is structured as follows: after a short overview of the theory of non-linear *sloshing* in par. 1.1, in Sec. 2 the mathematical model is discussed; Section 3 is dedicated to the numerical implementation and finally in Section 4 results related to several unsteady numerical simulations of the motion of a LO_2 and/or LH_2 propellant in a tank made of Aluminium-Lithium alloy (Al 2195) are presented: the main aim is the estimation of the pressures exerted by the sloshing fluid on the tank with the consequent stress field in the structure.

1.1 Theory of non-linear sloshing

The fluid motion in a partially filled tank forced to oscillate in a frequency domain close to its natural frequencies can be rather violent. The ratio between maximum free surface amplitude and characteristic tank motion amplitude is then high and significant non-linearities occur. The theoretical predictions by Faltinsen (Faltinsen et al., 2000) can be used as a basis for our studies. It is assumed that the tank is forced to oscillate with amplitude $L\,\varepsilon \sin \omega t$ in the horizontal x-direction. The non-dimensional parameter ε assumes usually values between 0 and 0.05 and it is defined in order to express the smallness of the motion. Let $\omega = 2\pi/T$ be the circular frequency of the excitation signal. The wave amplitude response A of the lowest primary mode and the excitation period T are coupled by a cubic secular equation:

$$\left[(T/T_1)^2 - 1\right](A/L) + m_1(A/L)^3 = P_1 H \tag{1}$$

where T_1 is the highest natural period of the tank, L is the tank width, H is the water depth, m_1 is a function of H/L and T/T_1. P_1H is a dimensionless excitation amplitude. It can be observed that this response is equal to the one of Duffing equation (Zeeman, 2000) and changes from soft-spring (decreasing amplitude with increasing frequency) to hard-spring (increasing amplitude with increasing frequency) behaviour as the ratio width–depth passes through a certain value, given by L/H =0.3374. Fig. 1 shows typical hard-spring behaviour.

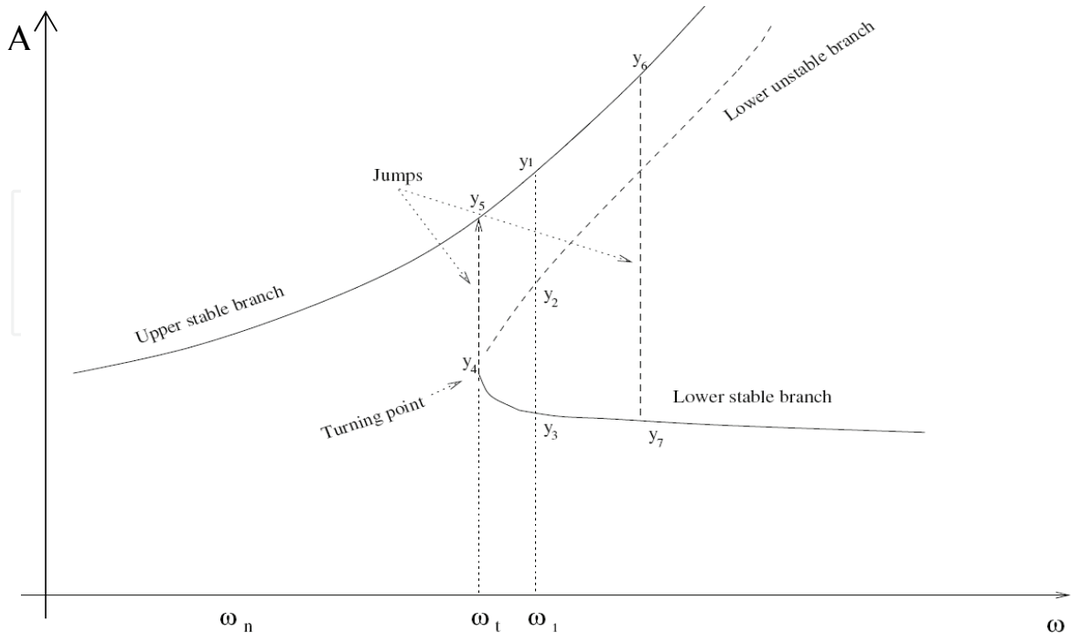

Fig. 1. The typical hard-spring behaviour

There exists a particular value of ω (i.e. ω t) such that the discriminant of the cubic equation is zero. For $\omega < \omega_t$ the secular equation has only one real root. For $\omega > \omega_t$ (e.g., ω_1) there will be three real valued solutions. What solution the physical system will select depends on how the value ω_1 is approached. If one starts to oscillate the tank with a much lower frequency, the solution will be y_1. If one does the opposite, the solution will be y_3. The physical system never select y_2 because it is an unstable solution. If we approach ω t from below and continue increasing ω, the solution will suddenly jump from y_6 to y_7. On the other hand, if one starts with a high frequency and decreases the frequency, the solution will follow the lower stable branch and suddenly jump from y_4 to y_5.

The first (upper) branch implies stable solutions. The second (lower) branch displays stable and unstable steady-state solutions with a turning point between them. The turning point defines a jump from the lower to the upper branch. Another jump from the upper to the lower jump occurs as A/L increases along the upper branch. It defines a downshift of maximum wave amplitude response. This pair of jumps constitutes the hysteresis between two stable solutions.

2. Mathematical model

2.1 Fluid dynamics

The evolutions of waves on the surface of a fluid enclosed in a box are described by means of the equations governing the motion of the flow with appropriate boundary conditions. As we are considering structures with characteristic dimensions larger than those of characteristic wavelengths, the viscous effects and surface tension have been neglected, whilst non-linear free surface effects have been taken into account. It has also been assumed that the amplitude of the oscillations is small if compared with the wavelength of the perturbation and with the depth of the box. All the physical quantities are referred to a

coordinate system rigid with the tank, so in the case of a moving tank the apparent forces must be taken into account. The equation governing the motion of an irrotational incompressible flow is the classical Laplace equation:

$$\nabla^2\phi = \frac{\partial^2\phi}{\partial x^2} + \frac{\partial^2\phi}{\partial z^2} = 0 \tag{2}$$

where ϕ is the potential velocity and the components of the velocity vector $\boldsymbol{u}(u,w)$ are given by:

$$u = \frac{\partial\phi}{\partial x} \quad w = \frac{\partial\phi}{\partial z} \tag{3}$$

Let $\eta(x,t)$ be the function describing the wave height measured with respect to the undisturbed configuration (Fig.2). The boundary conditions are imposed in the following way:

- on the rigid walls, the compatibility condition on the velocity field is:

$$\boldsymbol{u}\cdot\boldsymbol{n} = \boldsymbol{u}_s\cdot\boldsymbol{n}$$

where $\boldsymbol{n}$ is the outer normal to the boundary and $\boldsymbol{u_s}$ is the velocity deformation of the wall.

- on the free surface, a cinematic and a dynamic conditions are imposed. The first one states that the velocity of the surface must be equal to the vertical component of velocity:

$$\frac{\partial\eta}{\partial t} + \frac{\partial\phi}{\partial x}\frac{\partial\eta}{\partial x} - \frac{\partial\phi}{\partial z}_{(z=\eta)} = 0 \tag{4}$$

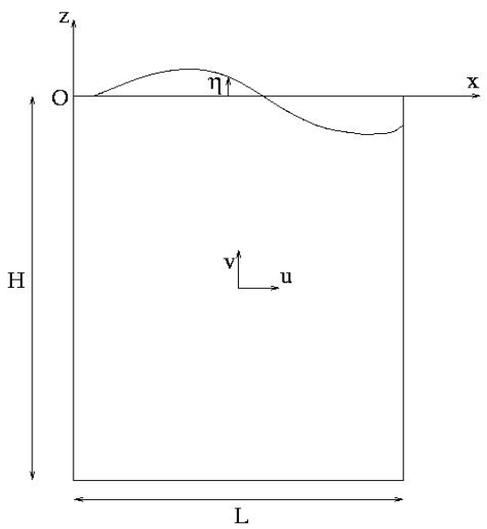

Fig. 2. Reference System for the Fluid

The dynamic condition states that the pressure on the free surface is equal to the external one (e.g., tank pressure). The Bernoulli theorem can be successfully used: if the volume

forces are reduced to the weight and the external pressure is set equal to zero, we obtain (Faltinsen et al., 2001):

$$\frac{\partial \phi}{\partial t} + \frac{1}{2}\left[\left(\frac{\partial \phi}{\partial x}\right)^2 + \left(\frac{\partial \phi}{\partial z}\right)^2\right] + g\eta + \frac{\partial \phi_c}{\partial t} = 0 \tag{5}$$

where g is the gravitational acceleration, $\frac{\partial \phi_c}{\partial t}$ is the acceleration of the tank with respect to an inertial coordinate system. This last term vanishes if the tank is motionless.
The Laplace equation and the boundary conditions have been set in non-dimensional form assuming the width of the tank L as reference length and a reference time equal to $(L/g_0)^{1/2}$ (g_0 is the gravity acceleration at earthly level). At the end of each time step, the liquid pressure on the solid walls is evaluated using the Bernoulli equation:

$$p = -\frac{\partial \phi}{\partial t} - \frac{1}{2}\left[\left(\frac{\partial \phi}{\partial x}\right)^2 + \left(\frac{\partial \phi}{\partial z}\right)^2\right] - gz - \frac{\partial \phi_c}{\partial t} \tag{6}$$

2.2 Structure

When the walls of a tank are thin, their vibrations under the effects of variable liquid pressure cannot be neglected. In this case it is essential to develop a mathematical model that keeps into account the deformations of the walls.
It is assumed that the tank is made up of an elastic isotropic material and that the constitutive law is the Hook's one.
The governing equations for the structure are the usual undefined equilibrium relations for continuous media. Under these hypotheses, a Finite Element discretization of the tank can be performed. If the displacement of the structure changes in the time, it is necessary to keep into account the inertial forces and the frictional resistances opposing the motion. These can be due to microstructure movements, air resistance etc. As a consequence, the equilibrium general condition for the structure in a Finite Element formulation assumes the following expression:

$$M\ddot{\vec{d}} + C\dot{\vec{d}} + K\vec{d} = f \tag{7}$$

where $\vec{d}$ is the displacement vector, M, C, K are respectively the mass matrix, the damping matrix and the stiffness matrix; f is the force vector. All the matrices are obtained by assembling related to each element (M^e, C^e and K^e). K^e is obtained according with reference (Golub et al., 1990) as:

$$K^e = \int_S B^T D B ds \tag{8}$$

where B is the strain-displacement matrix and D is the material matrix (depending on the Young modulus E and on the Poisson coefficient ν of the material). M^e is given by:

$$M^e = \int_S N^T \rho N ds \tag{9}$$

where ρ is the density and N is the shape function matrix. The definition of C^e is in practice difficult and therefore it is assumed that C^e is a linear combination of stiffness and mass matrices, that is:

$$C^e = \alpha M^e + \beta K^e \tag{10}$$

where α and β are determined experimentally.

3. Numerical methodology

The flowfield has been solved using a time-dependent algorithm, in order to obtain accurate true transient solutions. A Fully Implicit approach has been adopted for the time integration in order to guarantee high stability to the method. As shown in (Guj et al., 1993) this kind of approach represents a useful compromise among numerical efficiency, robustness and flexibility in applications. Particular care has been adopted for the treatment of the non-linear conditions on the free surface (Zienkiewicz et al., 1977) (Zienkiewicz et al., 1977). Linearization has been performed by *freezing* one of the terms at the previous time step.

$$\frac{\partial \eta}{\partial t} + \frac{\partial \phi^*}{\partial x}\frac{\partial \eta}{\partial x} - \frac{1}{2}\left(\frac{\partial \phi^*}{\partial z} + \frac{\partial \phi}{\partial z}\right) = 0 \tag{11}$$

$$\frac{\partial \phi}{\partial t} + \frac{1}{2}\frac{\partial \phi^*}{\partial x}\frac{\partial \phi}{\partial x} + \frac{1}{2}\frac{\partial \phi^*}{\partial z}\frac{\partial \phi}{\partial z} + \frac{1}{2}g(\eta + \eta^*) = -\frac{\partial \phi_c}{\partial t} \tag{12}$$

Where all the quantities are considered at the current time step, with the exception of the quantities marked with a * that are considered at the previous time step.
Few remarks can be made on this use of quantities evaluated at the previous time step. For what concerns the terms $\partial\phi/\partial z$ and η respectively in the first and second equation, the discrete form is obtained following the well known Cranck-Nicholson formula (Crank et al., 1947). Concerning the quadratic terms, since they are all non-linear, a linearization is required in order to approach the resulting algebraic problem with a linear solver. In this case one of the factors has been frozen at the previous time step, reducing the problem to a linear one (Galpin et al., 1986).
This technique guarantees a good coupling between all the equations.
As a result of the simplifying assumptions, the lack of viscosity may cause an undesirable contribution from the high frequency components to the numerical solution of the problem. This contribution is undesirable because the high frequency modes are poorly represented in the discretized system. As a consequence, a dispersion error may develop in the numerical solution. This effect may occur when the liquid is in the resonance zone or when the excitation level is relatively high. Numerical dissipation could be used to damp out the high frequency wave components propagating near the free surface, as proposed in (El-Zeiny, 2000). This strategy, however, has not been considered in the present work, as our goal is the investigation of the system for small amplitude oscillations. The Laplace equation has been discretized using a Finite Volume technique on a grid made up of quadrilateral elements. The computational grid is updated at each time step, in order to take into account the variation of the domain shape due to the movement of the free surface and of the solid walls. A transient procedure requires particular care, as the mass conservation could be

violated. The staggering of the variable location provides the maximum accuracy of the discretized derivatives and ensures the discrete conservation of mass at each time step. In fact, as shown in reference (Guj et al., 1993), it is possible to obtain mass conservation to round off error if the horizontal velocity is located at the middle of the vertical face of the computational cell and the vertical velocity is located at the middle of the horizontal face. As a consequence, the potential ϕ is naturally located at the centre of the cell.

For what concerns the boundary conditions, spatial derivatives are discretized using two-point backward differences, while time derivatives are discretized using three-point backward differences. At each time step the original system of partial differential equations gives rise to a large linear system of equations of the type $\boldsymbol{A}x=b$, where x is the unknown vector. The coefficient matrix $\boldsymbol{A}$ has a large sparse structure. The solution of this linear system via a direct method is not recommended due to the size of the problem, so an iterative procedure has been preferred: the Bi-CGSTAB algorithm (Van der Vorst, 1992) (Gluck et al., 2001), associated with a ILU decomposition of the matrix $\boldsymbol{A}$ as preconditioner has been employed. The Bi-CGSTAB algorithm is an iterative method belonging to the class of the Krylov subspace methods; it has been chosen for its good numerical stability and speed of convergence even in dealing with non-symmetric problems, as shown in references (Stella et al., 1996).

The spatial discretization of the structure has been performed using triangular elements with linear shape functions. The discretization of the time derivatives has been performed using Finite Difference approximations with a three-point formula for the second-order derivative and a two-point formula for the first-order derivative. Also in this case, the large sparse linear systems arising from discretization at each time step are solved using the Bi-CGSTAB algorithm without preconditioning.

3.1 Coupling between fluid and structural fields: the Multiphysics approach

Multiphysics (Bucchignani et al., 2008) is the science that simultaneously studies two or more different physical problems which interact dynamically. Each interacting physical entity is named *component*. The collection of the single components constitutes the *dynamical system* to be studied.

Other investigators (Felippa, 2001) prefer the term *coupled field problems*, by idealizing the interacting components as fields. Generally, the denomination *Multiphysics* tends to be applied to computational physics problem, whereas coupled field problems to mechanics.

The numerical simulation of components (or fields) of a system (or a coupled problem) as isolated entities has been pursued and refined within of each separate discipline. The challenge of these last years is to solve simultaneously the whole system in order to capture the physical effects arising from the interaction. This approach requires innovative mathematical modelling, new numerical methods and a strong interdisciplinary approach.

The fields of a coupled problem are usually governed by partial differential equations in space and time. Three approaches to the time advancing of the whole system can be followed:

1. **Elimination:** At each time step one or more fields can be eliminated by appropriate techniques such as integral transform, and the remaining component solved by a standard time integration scheme.
2. **Partitioned integration:** The system components are treated as isolated entities which separately advance in time. Interaction effects are viewed as *forcing effects* during the time advancing. This approach can be of two types:

- **Loose or weak coupling.** Data generated by a system during its time advancing are used as input data from the other(s) system (one way interaction)
- **Tight or strong coupling:** At each time step data generated by the single systems are exchanged among them (mutual interaction).

3. **Monolithic or simultaneous integration:** The whole system is treated as monolithic entity, that is the fields are coupled at the fundamental equation level and advance simultaneously in time.

The methodology proposed here for the solution of the fluid-structure interaction problems is based on a partitioned approach with a strong coupling. One of the advantages of the Partitioned methods is the software reuse to solve each field involved in the simulation (Felippa et al., 2001), whereas a monolithical approach requires the development of an unified mathematical model and therefore a dedicated software.

Another important advantage in the specific case is that a partitioned treatment preserves the different approaches used for CFD, that is based on an "eulerian" formulation, and Computational Structural Dynamics (CSD), which adopts a "Lagrangian" point of view.

The coupling between fluid and structure is obtained by using a semi-implicit *staggered algorithm* (Felippa et al., 2001) (Matthies et al., 2003).

A staggered method introduces an external (physical) time loop and considers the two solvers as partitions or sub-systems of the whole system to be solved. They can be classified as follows: explicit, when both solvers use the values computed at the previous time step; semi-implicit, when one of the two subsystems uses the values computed by the other solver; implicit, when both solvers use the values at the current time. In the latter case some linearization procedures have to be used.

In the applications of interest, there are other important problems to be considered, such as the data transfer between the different grids, the fluid domain deforming, which could be well represented by an ALE formulation, the relationship between the external time step and those used by each solver, which are limited by their stability regions.

Structural motions are typically dominated by low frequency vibration modes, which means that large time step can be used. On the other hand, the thermo fluid dynamics response must be captured in a smaller time scale because of unsteady effects involving shock, vortices, turbulence and chemical reactions. Thus, the use of a smaller time step for the fluid is natural. This device is called sub-cycling. The ratio of structural to fluid time steps may range from 10:1 through 1000:1, depending on the problem characteristics and the use of explicit or implicit fluid solver (Strain, 1999).

The semi-implicit staggered approach proposed in this work can be illustrated as follows:

do n= 1, ntime
| Call **fluid** (F(n-1),S(n-1),F(n))
| Call **transf**
| Call **struct** (S(n-1), F(n),S(n)
| Call **grid_deforming**
End do

where **fluid** and **struct** represent, respectively, the fluid and the structural solvers, **transf** the subroutine for the data transfer between fluid and structural fields and **grid-deforming** the subroutine which updates the fluid domain on the basis of the solid deformations. Details about these subroutine are given in the following.

As described above, in a general approach the CFD and CSD solvers use different formulations and discretizations. The two computational grids are not continuously interconnected, in the sense that the nodes on the interface of the fluid domain do not coincide with the ones of the interface of the solid domain (see Fig.3). Therefore, the data exchange between the two solvers is not immediate, but requires some interpolation operations. The data transfer from CFD to CSD is realized by evaluating the forces acting on the nodes of the solid interface starting from the values of the pressure in the nodes of the liquid interface. This operation must be performed carefully, in such a way that the global energy of the system is conserved.
To this end it is worth nothing that the lateral sloshing of liquid propellant in a tank results in a distributed pressure loading on the walls, which is of importance for detailed structural design. Indeed, the forces acting on the CSD nodes are:

$$F_i = \int_S -N_i p_i n ds \tag{13}$$

where the pressure p_i in the CSD nodes is the integral of the liquid pressure on the faces of the CSD cells (Fig.4):

$$p_i = \frac{1}{\Delta x} \int_{x_i - \Delta x/2}^{x_i + \Delta x/2} p(x) dx \tag{14}$$

Otherwise, in many practical problems the liquid pressure distribution is rather regular and so it is convenient to have an analytical representation of the pressure distribution by means of a polynomial interpolation; in this case a second-order polynomial is adopted.

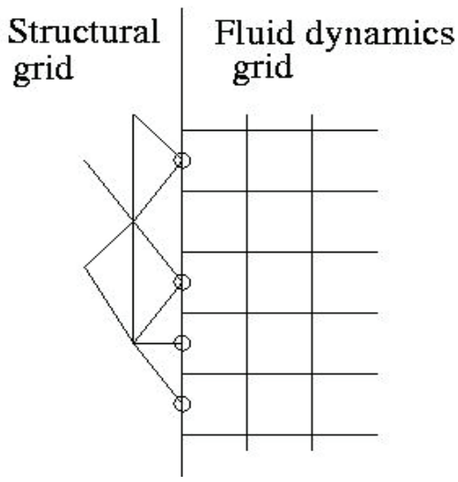

Fig. 3. Solid-fluid interface

The data transfer from CSD to CFD is less difficult and is performed by a simple data interpolation on the deformations. This is due to a better regularity of the physical phenomenon of structural deformation with respect to the pressure fluctuations.
The time-stepping algorithm works as follows. First, the partition method that we have developed performs a fluid dynamics simulation and the pressures on the solid walls and

displacements of the points of the free surface are evaluated. Then, data are transferred to the CSD solver and the structural simulation is performed, in order to evaluate the deformations of the tank. These values are transferred to the CFD solver to update the boundary conditions. Besides, it is now possible to draw the new shape of the CFD domain and to update the computational grid, performing a new time step and continuing the time marching procedure with a new CSD simulation (performed on the grid which has been updated on the basis of the previous deformations).

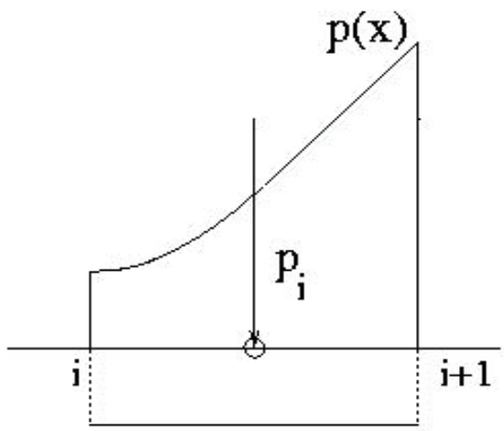

Fig. 4. Pressure distribution on a cell face

4. Numerical results

As practical applications, several unsteady numerical simulations of the motion of a LO_2 and/or LH_2 propellant in a tank made of Aluminium-Lithium alloy (Al 2195) have been performed in order to estimate the pressures exerted by the sloshing fluid on the tank with the consequent stress field in the structure.

It is worth nothing that LO_2 and LH_2 propellant have been chosen considering that for RLV the higher thrust-to-weight ratio of other propellants such as LO_2-Kerosene are offset by their lower specific impulse, which leads to a higher propellant demand, higher launch mass and hence to a higher residual propellant.

The reentry trajectory, provided in Fig. 5, has been considered as a typical RLV flight scenario to take into account in the numerical simulations.

Among the specific critical issues that can be envisaged within RLV design, two basic ones are of general interest in the framework of fluid-structure interaction. They are:

1. the propellant management, since it influences the operability of a RLV considering the automatic fly-back and landing needs. Indeed, a large quantity of propellants filling the tanks determines high safety constraints.
2. the alternative between an aeroshell or loads-carrying tanks structures may heavily affect the vehicle design in terms of: launch mass, complexity, safety and operability. Therefore, it can be influence sloshing analysis.

The post-MECO propellant management issue is even more important in case of mission abort, since the time available to expel the residual propellant in atmosphere may be extremely short.

4.1 RLV reentry flight scenario

Figure 5 shows the nominal reentry scenario investigated to assess the fluid-structure interaction issue (Spies, 2003).

The RLV mission starts from launch site, where the two-stage-to-orbit (TSTO) vehicle lifts-off with all the engines running. Hence the upper stage separates from the booster and after MECO, it transports the payload into the final target orbit. At the end of mission, the reusable launcher follows a gliding downrange re-entry flight to a landing site.

When entering the densest layers of the atmosphere, the aerodynamic forces rapidly increase and, finally, stabilize the vehicle attitude at an angle of attack of about 30÷40 deg. In this trajectory phase, certain constraints typically apply. For instance, the dynamic pressure is confined below certain limits, the heat flux at stagnation point does not exceed the allowable value for the vehicle thermal protection system (TPS), the total load factor is smaller than the one bearable by the launcher structure design, etc. Those trajectory constraints identify the admissible flight envelope, well known as reentry corridor of the RLV, thus defining the most severe dimensioning criteria of the launcher.

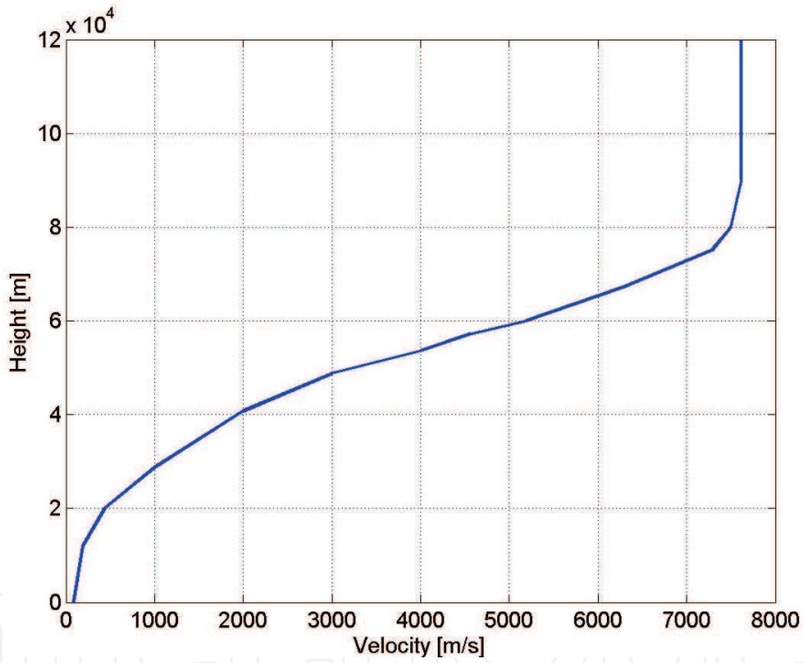

Fig. 5. Typical RLV re-entry trajectory in the Altitude-velocity map (Spies, 2003)

During reentry, the launcher decelerates taking advantage of aerodynamic forces (e.g., lift and drag) by flying at an angle of attack (AoA) α, thus performing a gliding descent.

The free body diagram of the RLV is recognized in Fig.6.

Then, at the peak deceleration region, it must be noted that by imposing the equilibrium both in the axial (A) and lateral (L) direction, it results that:

$$\begin{cases} A_A = \left|\vec{a}_A - \vec{g}\, sen\varphi\right| \cong \left|(0.1 \div 0.3)\vec{g}_o\right| \\ \\ A_L = \left|\vec{a}_L + \vec{g}\cos\varphi\right| \cong \left|(2.0 \div 3.0)\vec{g}_o\right| \end{cases} \tag{15}$$

where the value of the gravity acceleration at the flight altitude H is determined according with the well known formula:

$$g = g_0 \left(\frac{R_{Earth}}{R_{Earth} + H} \right)^2 \tag{16}$$

where g_o is sea level acceleration (e.g., 9.81 m/s^2), R_{Earth} is the Earth's radius (e.g., 6378 km). Note that, the gliding descent helps to mitigate the acceleration environment that the vehicle has to withstand during descent.

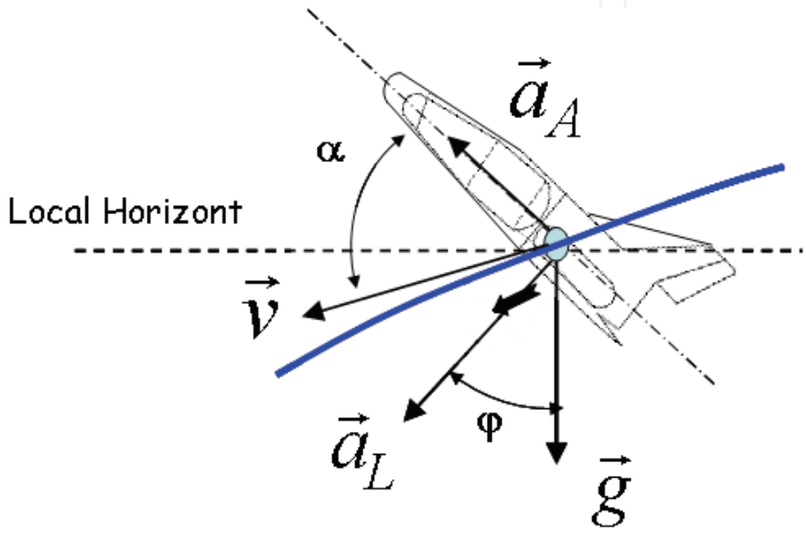

Fig. 6. Typical RLV free body diagram

So, as the lowest sloshing frequency corresponds to the lateral excitation of the tank (lateral sloshing), the design considerations are generally governed by the lateral slosh (NASA, 1968). In this case the linear theory of sloshing in rigid tanks states that, on the tank is applied a time dependent pressure, which is a function (f_1) of:

$$p = f_1(p_{Tank}, y, \rho\eta A_A \sin\omega t) \tag{17}$$

where ω is the fundamental lateral frequency (sloshing frequency), p_{Tank} is the tank pressurization, ρ is the fluid density, and y is the free-surface height.

For a rigid cylindrical tank, the second-mode sloshing mass is only about few percent of the first-mode sloshing mass; therefore, the second and higher mode sloshing effects are generally negligible (NASA, 1968). This means that the resulting fluid force decreases rather substantially in the higher modes of oscillation.

In particular, in the case of rigid cylindrical tank with a flat bottom, the frequency rad/s of free-surface motion is a function (f_2) of:

$$\omega_n = f_2 \left(\varepsilon_n \frac{h|\vec{a}_A|}{R_{Tank}} \right) \tag{18}$$

where ε_n is a coefficient that take into account for the slosh mode, h is the height of quiescent fluid surface and R_{Tank} is the tank radius. For example, when $h>>R_{Tank}$ we have that (NASA, 1968):

$$\omega_n \cong \sqrt{\varepsilon_n \frac{|\vec{a}_A|}{R_{Tank}}} \tag{19}$$

Moreover, Eq. (19) can be used to estimate the natural sloshing frequency of tanks of many other shapes, filled to various heights (NASA, 1968).
For what concerns numerical simulations, the test cases presented herein assume that the undeformed tank and flow are the ones shown in Fig. 7 (Bucchignani et al., 2008).
The external dimensions are L=5 m and H=1 m in the case of LO_2 tank while L=15 m and H=3 m for the LH_2 tank. The walls are made up of Al 2195 (e.g., Young module: E=84000 MPa at 20 K, 83100 MPa at 80 K, and 76000 MPa at 300 K; Poisson module: ν=0.33, and density ρ_{Al2195}=2700 Kg/m^3) and are characterized by a thickness section s=0.1 m (LO_2) and s=0.3 m (LH_2). The frictional resistance opposing the motion is neglected. The density of LO_2 is ρ_{LO2}=1300 Kg/m^3, while the one of LH_2 is ρ_{LH2}=3 Kg/m^3.
The fluid dynamics domain, in the undisturbed configuration, ranges from 0.1 m to 4.9 m in the horizontal direction, and from 0.1 m to 0.8 m in the vertical direction for the LO_2 sloshing.

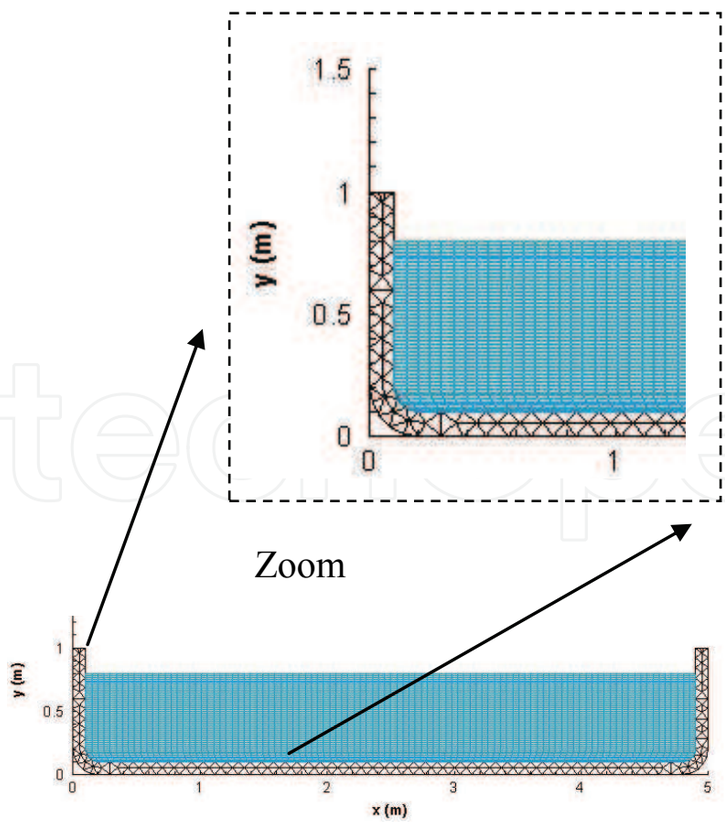

Fig. 7. The computational grid for the structure-flow in the case of LO_2 test case

For the CFD solver, a grid with 101 by 51 nodes has been adopted, while for the CSD solver an unstructured grid of 238 nodes and 312 elements is used. These grids (undisturbed configurations - see Fig.7) have been generated by means of the commercial code ANSYS ICEM CFD 10.
The time step is set equal to 10^{-3} (non-dimensional units).
Figure 8 shows the deformed grid as evaluated automatically by the code during the time stepping.

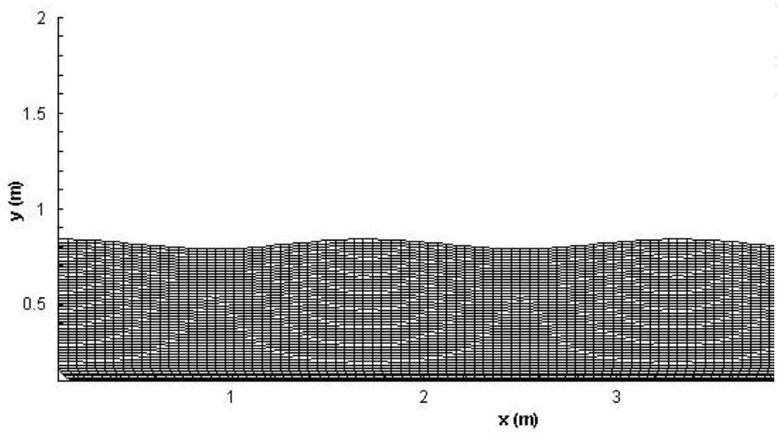

Fig. 8. The computational grid for the fluid

The deviation with respect to tank pressure p_{Tank}=120 kPa for $\omega=2\pi$ is recognized in Fig. 9 (up) and Fig. 9 (down) for LO_2 and LH_2 simulation, respectively. These results refer to the time t=3 [min].

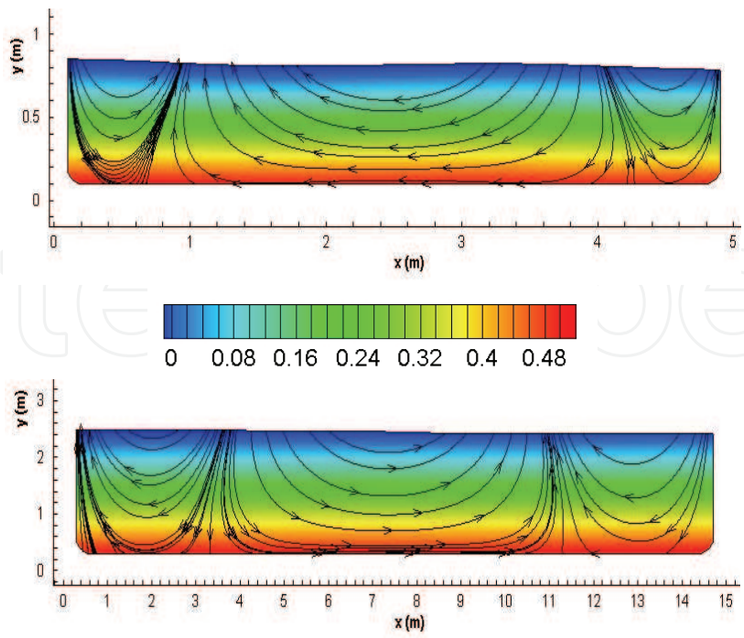

Fig. 9. Streamlines at a fixed time step superimposed on the pressure field in the plane of oscillation. LO_2 simulation (up) and LH_2 (down)

This distributed pressure loading on the walls is of importance for detailed structural design, since it resulted in a stress field in the tank structure, as recognized in Fig. 10 for the case of LH_2, and in Fig.11 for the case of LO_2 (Bucchignani et al., 2008).

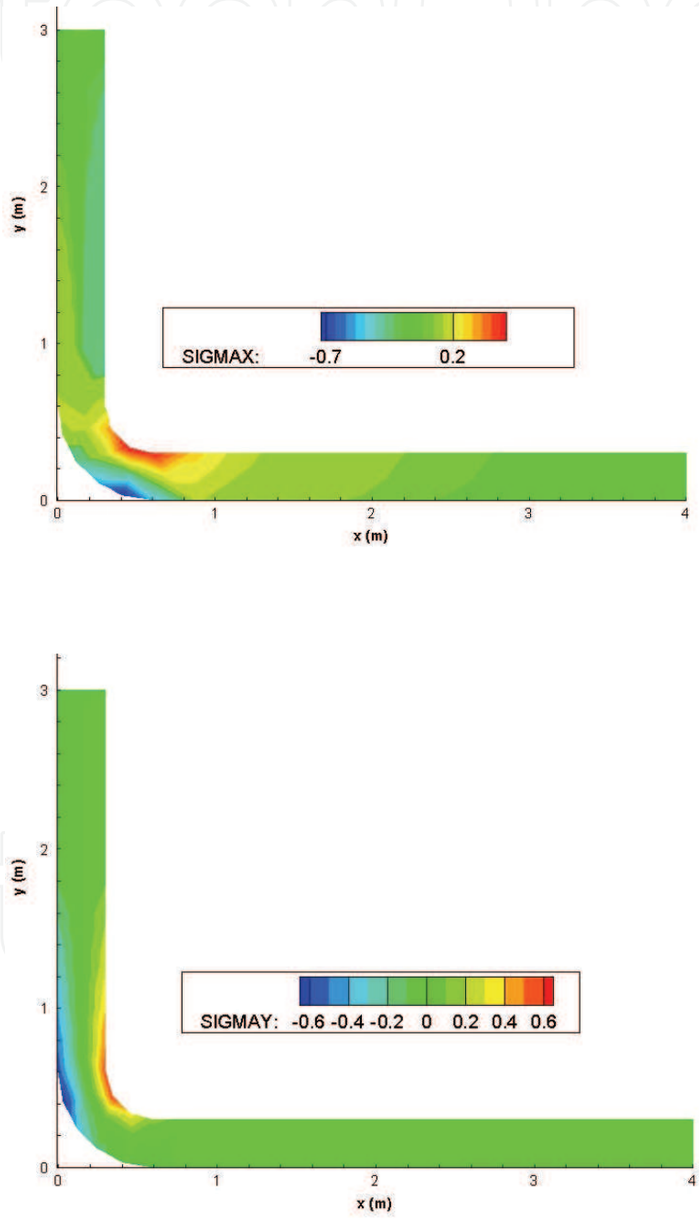

Fig. 10. σ_X and σ_Y tensions field (MPa) in the plane of oscillation. LH_2 simulation

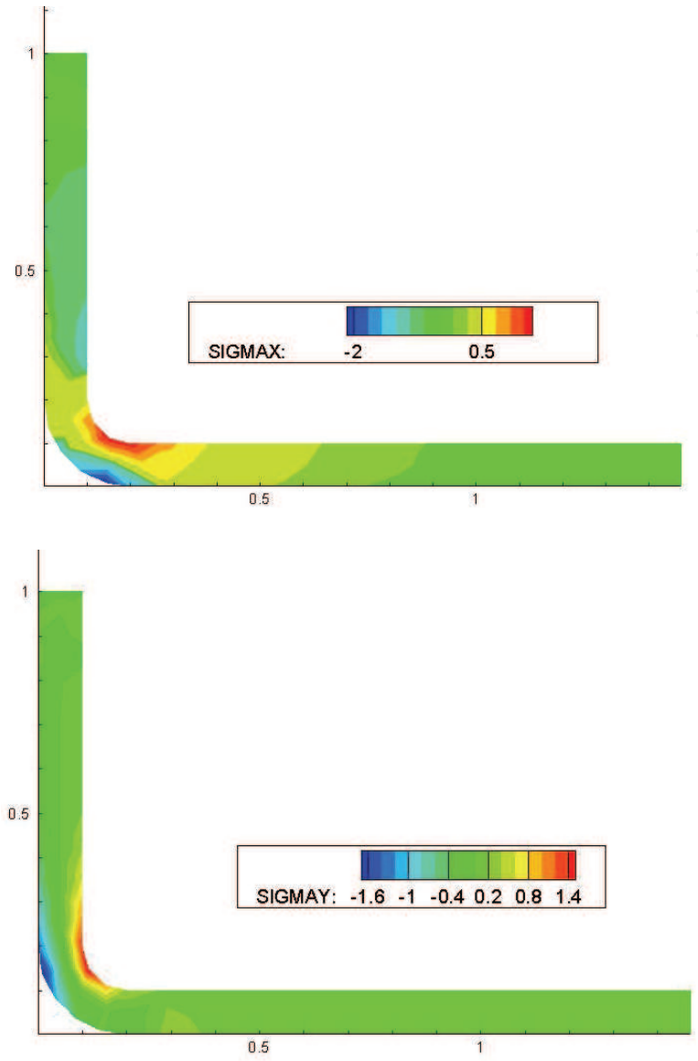

Fig. 11. σ_X and σ_Y tensions field (MPa) in the plane of oscillation. LO_2 simulation

5. Conclusions

A software environment for the analysis of coupled liquid-structure fields has been developed. A staggered partitioned procedure has been employed using finite volume (FV) for the fluid and finite element (FE) for the structure.

A tank configuration typical of RLV has been considered. It is filled with liquid propellant such as LH_2 and/or LO_2. Stress distributions in the structure and flow field in the liquid phase have been shown as well as transient history of structure displacement. Maximum stress as a function of maximum acceleration has also been shown and compared with structure limit.

In the future, it is our intention to implement a sub-cycling strategy in order to reduce the computational time, and to develop a fully implicit staggered scheme based on a Newton-Krylov algorithm.

6. References

Bucchignani, E., Stella, F., Paglia F. (2004). A Partition method for the solution of a coupled liquid structure interaction problem. *Applied Numerical Mathematics,* Vol. 51, No. 4, page numbers (463-475), ISSN:0168-9274.

Bucchignani, E.; Pezzella, G.; Matrone, A. (2008). Numerical Simulation of Liquid-Structure Interaction Problems in a Tank for Aerospace Applications. *Sixth European Symposium on Aerothermodynamics for Space Vehicles.* Palais des Congrès, Versailles, France. 3-5 November 2008.

Cranck, J.; Nicholson, P. (1947). A practical method for numerical evaluation of solutions of partial differential equations of the heat conduction type, Proc. *The Cambridge Philosophical Soc*. Vol. 43, No. 50, page numbers (50-67).

El-Zeiny, A. (2000). Nonlinear Time-Dependent Seismic Response of Unanchored Liquid Storage Tanks, PhD Thesis, Irvine, University of California, 2000.

Faltinsen, O. (1974). A nonlinear theory of sloshing in rectangular tanks, *Journal of Ship Research*. Vol. 18, No. 4, page numbers (224–241).

Faltinsen, O.; Rognebakke, O.; Lukowsky, I.; Timokha, A. (2000). Multidimensional modal analysis of nonlinear sloshing in a rectangular tank with finite water depth. *Journal of Fluid Mechanics*. Vol. 407, page numbers (201–234).

Faltinsen, O.; Timokha, A. (2001). An adaptive multimodal approach to nonlinear sloshing in a rectangular tank. *Journal of Fluid Mechanics*, Vol. 432, page numbers (167-200). ISSN:0022-1120.

Felippa, C.A.; Park, K.C.; Farhat, C. (2001). Partitioned analysis of coupled mechanical systems, *Computer methods in applied mechanics and engineering*, Vol. 190, No. 24-25, page numbers (3247-3270). ISSN: 0045-7825.

Galpin, P.F.; Raithby, G.D. (1986). Treatment of non-linearities in the numerical solution of the incompressible Navier-Stokes Equations. *International Joural of Numerical Methods in Fluids*. Vol. 6, No. 7, page numbers (409-426).

Gluck, M.; Breuer, M.; Durst, F.; Halfmann, A.; Rank, E. (2001). Computation of fluid-structure interaction on lightweight structures, *Journal of Wind Engineering and Industrial Aerodynamics,* Vol. 89, page numbers (1351-1368). ISSN:0167-6105.

Golub, G.; van Loan, C. (1990). *Matrix computations*, The John Hopkins University Press. Baltimore, Maryland 21218-4363. ISBN:0-8018-5414-8.

Guj, G.; Stella, F. (1993). A Vorticity-Velocity method for the numerical solution of 3D incompressible flows, *Journal of Computational Physics*, Vol. 106, No. 2, June 1993, page numbers (286-298). ISSN: 0021-9991.

Matthies, H. G.; Steindorf, J. (2003). Partitioned Strong coupling algorithms for fluid-Structure Interaction., *Computers and Structures*, Vol. 81, No. 8-11, page numbers (805-812)

NASA (1968). Propellant slosh loads. *NASA SP-8009*.

Spies, J. (2003). RLV Hopper: Consolidated System Concept, *Acta Astronautica*. Vol. 53, No. 4, page numbers (709-717). ISSN: 0094-5765.

Stella, F.; Bucchignani, E. (1996). True transient vorticity-velocity method using preconditioned Bi-CGSTAB, *Numerical Heat Transfer Part B*. Vol. 30, page numbers (315-339).

Strain (1999). Three Methods for Moving Interfaces. *Journal of Comp. Physics*, 151, page numbers (616-648).

Van der Vorst, H. (1992). Bi-CGSTAB, a fast and smoothly converging variant of Bi-CG for the solution of nonsymmetric linear systems, SIAM *J. Sci. Stat. Comput*. Vol. 13, No. 2, page numbers (631-644).

Zienkiewicz, O.; Taylor, R.L. (1977). *The Finite Element Method Vol.1*, McGraw-Hill Book Company.

Zienkiewicz, O.; Taylor, R.L. (1991). *The Finite Element Method Vol.2* (Fourth Edition), McGraw-Hill Book Company.

Zeeman, E. (2000). Duffing's equation: catastrophic jumps of amplitude and phase, Lectures available at: http://www.math.utsa.edu/~gokhman/ecz/duffing.html.

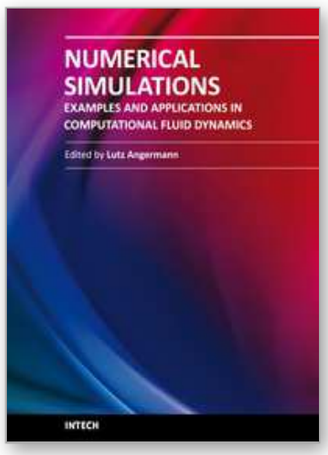

Numerical Simulations - Examples and Applications in Computational Fluid Dynamics

Edited by Prof. Lutz Angermann

ISBN 978-953-307-153-4
Hard cover, 440 pages
Publisher InTech
Published online 30, November, 2010
Published in print edition November, 2010

This book will interest researchers, scientists, engineers and graduate students in many disciplines, who make use of mathematical modeling and computer simulation. Although it represents only a small sample of the research activity on numerical simulations, the book will certainly serve as a valuable tool for researchers interested in getting involved in this multidisciplinary ï¬eld. It will be useful to encourage further experimental and theoretical researches in the above mentioned areas of numerical simulation.

How to reference

In order to correctly reference this scholarly work, feel free to copy and paste the following:

Edoardo Bucchignani, Giuseppe Pezzella and Alfonso Matrone (2010). Numerical Simulation of Liquid-Structure Interaction Problem in a Tank of a Space Re-Entry Vehicle, Numerical Simulations - Examples and Applications in Computational Fluid Dynamics, Prof. Lutz Angermann (Ed.), ISBN: 978-953-307-153-4, InTech, Available from: http://www.intechopen.com/books/numerical-simulations-examples-and-applications-in-computational-fluid-dynamics/numerical-simulation-of-liquid-structure-interaction-problem-in-a-tank-of-a-space-reentry-vehicle

INTECH
open science | open minds

InTech Europe
University Campus STeP Ri
Slavka Krautzeka 83/A
51000 Rijeka, Croatia
Phone: +385 (51) 770 447
Fax: +385 (51) 686 166
www.intechopen.com

InTech China
Unit 405, Office Block, Hotel Equatorial Shanghai
No.65, Yan An Road (West), Shanghai, 200040, China
中国上海市延安西路65号上海国际贵都大饭店办公楼405单元
Phone: +86-21-62489820
Fax: +86-21-62489821

IntechOpen